BIOCHEMISTRY
including biophysical chemistry & molecular biology

Article

pubs.acs.org/biochemistry

The SNARE Motif of Synaptobrevin Exhibits an Aqueous−Interfacial Partitioning That Is Modulated by Membrane Curvature

Binyong Liang,[‡] Damian Dawidowski,[§] Jeffrey F. Ellena,[†] Lukas K. Tamm,*[,‡] and David S. Cafiso*[,‡,§]

[†]Biomolecular Magnetic Resonance Research Core, University of Virginia, P.O. Box 800741, Charlottesville, Virginia 22908, United States

[‡]Department of Molecular Physiology and Biological Physics, Center for Membrane Biology, University of Virginia, P.O. Box 800886, Charlottesville, Virginia 22908, United States

[§]Department of Chemistry, University of Virginia, McCormick Road, Charlottesville, Virginia 22904, United States

Supporting Information

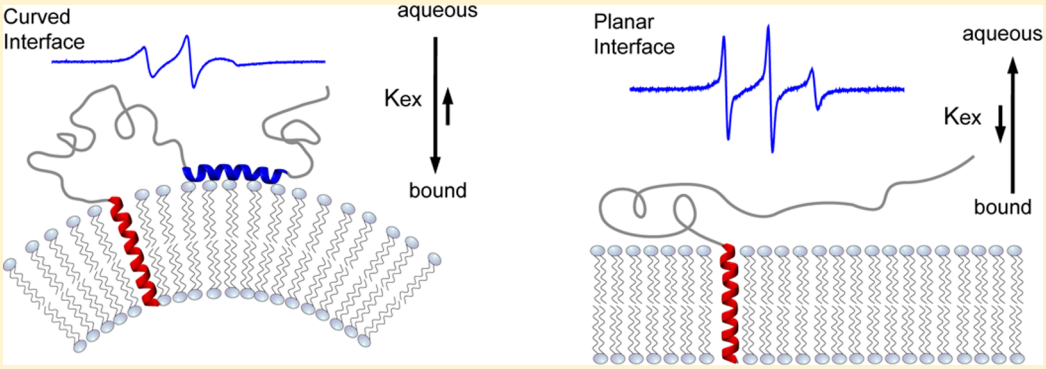

ABSTRACT: The structure and interfacial association of the full-length vesicle SNARE, synaptobrevin, were compared in four different lipid environments using nuclear magnetic resonance and electron paramagnetic resonance spectroscopy. In micelles, segments of the SNARE motif are helical and associated with the interface. However, the fraction of helix and interfacial association decreases as synaptobrevin is moved from micelle to bicelle to bilayer environments, indicating that the tendency toward interfacial association is sensitive to membrane curvature. In bilayers, the SNARE motif of synaptobrevin transiently associates with the lipid interface, and regions that are helical in micelles are in conformational and environmental exchange in bicelles and bilayers. This work demonstrates that the SNARE motif of synaptobrevin has a significant propensity to form a helix and exchange with the membrane interface prior to SNARE assembly. This transient interfacial association and its sensitivity to membrane curvature are likely to play a role in SNARE recognition events that regulate membrane fusion.

Neurotransmitter release results from a membrane fusion event that joins the synaptic vesicle membrane with the presynaptic plasma membrane. This fusion event is driven by soluble *N*-ethylmaleimide-sensitive factor attachment receptor proteins (SNAREs), which form the core of the membrane fusion machinery. SNAREs assemble into a tight four-helix bundle that is thought to provide the energy required to overcome the barrier to fusion,[1,2] and in the neuronal system, the SNARE complex is formed from syntaxin 1a and SNAP-25 on the plasma membrane and synaptobrevin 2 in the vesicle membrane. The regulation and assembly of these proteins into the SNARE complex is essential to neuronal fusion, and a number of critical effector proteins that function to mediate this process have been identified.[3−5] In the case of syntaxin, Munc18-1 is believed to control the configuration of syntaxin and thereby regulate its ability to assemble into the SNARE complex.[3−5] Less is known about the state of the vesicle-associated SNARE protein, synaptobrevin 2, which is generally thought to be unstructured prior to the SNARE assembly process.

The extravesicular SNARE domain of synaptobrevin 2 (syb) encompasses residues 30−85 and is anchored to the membrane of synaptic vesicles through a single transmembrane helix near its C-terminal end (residues 95−116). In the absence of the transmembrane domain, synaptobrevin is reported to be almost completely unstructured in solution.[6,7] However, a high-resolution nuclear magnetic resonance (NMR) study of full-length syb in dodecylphosphocholine (DPC) micelles[8] indicated that stretches of the SNARE motif are helical. This micelle structure is shown in Figure 1a. The N-terminal half of the SNARE motif (residues 36−54), the juxtamembrane coupling region (residues 77−88), and the transmembrane domain (residues 93−115) are α-helical, while the remainder of

Received: December 6, 2013
Revised: February 13, 2014
Published: February 19, 2014

   dx.doi.org/10.1021/bi401638u | *Biochemistry* 2014, 53, 1485−1494

the protein is unstructured. The SNARE motif is also observed to be partially helical for syb lacking the transmembrane anchor in the presence of DPC micelles; however, helical content is not observed for the soluble fragment in the absence of DPC micelles, confirming the earlier studies. The work in micelles indicates that syb has a substantial α-helical structure in selected regions, which might play a role in protein−protein recognition and the nucleation of SNARE complex formation. In contrast, a more recent study of full-length syb in nanodiscs and in phospholipid bilayers indicates that residues 1 to ∼75 are unstructured while the transmembrane domain of syb was not resolved.[9] This suggested that the helical content found in DPC may be induced by the micelle environment, producing helical structure in the SNARE motif and an interfacial association that may not occur in more nativelike environments.

In this work, we examine the structure and configuration of syb using both NMR and EPR spectroscopy in bilayer and bicelle environments and compare the result with that found previously by NMR in DPC micelles. In agreement with a more recent study,[9] we find that DPC micelles induce helical structure and interfacial association of the SNARE motif when compared to more native environments such as bilayers and bicelles. However, NMR spectroscopy demonstrates that in bicelles, syb is in conformational exchange and that some residual helical content is present. Moreover, EPR spectroscopy from 21 sites along syb provides strong evidence that even in a lipid bilayer, the SNARE motif of syb exchanges between aqueous and membrane environments. Although the SNARE motif is largely disordered, segments of the SNARE motif transiently associate with lipid bilayers, and this association is enhanced as one proceeds from bilayer to bicelle and micelle environments. Thus, the interfacial association and structure that are seen in DPC micelles persists in lipid bilayers, although to a greatly reduced extent. Our results suggest that the larger helical content and membrane association that occurs in micelles versus bilayers are a result of the sensitivity of amphipathic regions of the SNARE domain to interfacial defects and the curvature of the interface. The transient interfacial association and/or helix formation in the SNARE-forming motif of syb may modulate the availability of synaptobrevin and its ability to assemble into the SNARE core complex.

EXPERIMENTAL PROCEDURES

Protein Expression and Bicelle Sample Preparation. Syb(1−116) from *Rattus norvegicus* was expressed in BL21-(DE3) cells under the control of the T7 promoter (pET28a) and purified as described previously.[10,11] The QuikChange polymerase chain reaction method (Agilent Technologies, Wilmington, DE) was used to introduce single-cysteine mutations into syb. Synaptobrevin mutants for EPR spectroscopy were expressed in lysogeny broth (LB) medium with 40 mg/L kanamycin. When the cells reached a cell density of 0.8−1.0, expression was induced with 0.4 mM isopropyl thio-β-galactoside. The cells were incubated at 20 °C overnight and then harvested by centrifugation at 3500*g*. For NMR measurements, isotope labeling was accomplished in EMBL medium in 100% D_2O supplemented with $(^{15}NH_4)_2SO_4$, ^{13}C-labeled glucose, and ^{2}H-, ^{13}C-, and ^{15}N-labeled 10% Bioexpress. For both EPR and NMR spectroscopy, syb was purified in the presence of 1% sodium cholate and exchanged into 0.1% dodecylphosphocholine (DPC) while bound to a Ni affinity column. The eluted protein from the Ni affinity column was concentrated and then digested at 4 °C overnight by thrombin to remove the six-His tag.

To make bicelle samples for NMR measurements, detergent exchange and buffer exchange were conducted via size-exclusion chromatography (Superdex200 10/300 column) with a pH 6.5 buffer containing 1% dihexanoylphosphatidylcholine (DHPC), 20 mM bis-tris, 50 mM NaCl, 5 mM DTT, and 1 mM EDTA. Only the major peak, but not the trailing shoulder, was collected and then concentrated to ensure the separation of DPC-bound syb from DHPC-bound syb. DHPC concentrations usually varied between 150 and 300 mM in the final concentrated syb/DHPC sample. One-dimensional NMR was employed to accurately determine the DHPC concentrations in such samples by comparing the detergent acyl proton signals against corresponding resonances in a series of standard DHPC samples. On the basis of the measured DHPC concentrations, amounts of dimyristoylphosphatidylcholine (DMPC) corresponding to predetermined bicelle q factors were dispensed from a chloroform stock and dried under vacuum overnight. After the syb/DHPC sample had been mixed with the dried DMPC lipid film, homogeneous bicelle sample were achieved by multiple steps of freezing and thawing.[12] Multiple bicelle samples with q factors that vary from 0.25 to 0.5 were employed, and they were stable for a few months at a measuring temperature of 40 °C.

NMR Spectroscopy. TROSY versions[13] of three-dimensional backbone experiments [HNCA,[14] HNCACB,[15] HNCO,[14] and HN(CA)CO[16]] with [^{2}H,^{13}C,^{15}N]Syb(1−116) in q = 0.33 bicelles (66 mM DMPC and 200 mM DHPC) were conducted on a Bruker Avance 800 MHz spectrometer equipped with a cryoprobe. Secondary chemical shifts were evaluated as described previously:[17] $(\Delta C\alpha - \Delta C\beta)_i$ was calculated as $^{1}/_{3}(\Delta C^{\alpha}_{i-1} + \Delta C^{\alpha}_{i} + \Delta C^{\alpha}_{i+1} - \Delta C^{\beta}_{i-1} - \Delta C^{\beta}_{i} - \Delta C^{\beta}_{i+1})$. NMR dynamics measurements, including heteronuclear[12] ^{15}N NOE, ^{15}N T_1, and ^{15}N T_2 measurements,[18] were also collected at 800 MHz. A 5 s saturation delay was used in the heteronuclear NOE experiment. Relaxation delay times of 10, 30, 70, 150, 300, 600, 1000, and 1500 ms and 0, 17, 51, 68, 119, 170, 238, and 494 ms were employed in the T_1 and T_2 experiments, respectively.

For CPMG relaxation dispersion experiments, bicelle samples with q values from 0.25 to 0.5 were employed at temperatures from 15 to 40 °C to determine the optimal conditions for such measurements. Although the relaxation behavior changes only slightly, the general trend is consistent throughout the surveyed conditions. Typically, the TROSY versions of CPMG relaxation dispersion experiments[19] were conducted on a Bruker Avance 600 or 800 MHz spectrometer. $R_{2,\mathrm{eff}}$ was calculated on the basis of the equation[20]

$$R_{2,\mathrm{eff}} = -\frac{1}{T_{\mathrm{CP}}} \ln \frac{I(\nu_{\mathrm{CPMG}})}{I_0}$$

where $I(\nu_{\mathrm{CPMG}})$ and I_0 are peak intensities measured with and without the applied 40 ms constant time CPMG element, T_{CP}, respectively. Redundant measurements were performed to estimate standard deviations. Effective fields, ν_{CPMG}, as defined by $^{1}/_{4}\tau_{\mathrm{CPMG}}$, ranged from 25 to 1000 Hz, where $2\tau_{\mathrm{CPMG}}$ was the time between the centers of two consecutive 180° pulses.

All spectra were processed and analyzed with NMRPipe[21] and Sparky.[22] Indirect dimensions in the three-dimensional experiments were processed with forward−backward linear prediction.

Sample Preparation and EPR Measurements. The spin-labeled side chain R1 was attached to selected sites on syntaxin by adding 1 mg of 1-oxyl-2,2,5,5-tetramethyl-3-pyrro-line-3-methyl methanethiosulfonate (MTSL) (Santa Cruz Biotechnology, Dallas, TX) in ethanol to the isolated cysteine-containing protein and incubating the mixture overnight at 4 °C. The unbound spin-label was then removed using a HiPrep 26/10 desalting column (GE Healthcare, Piscataway, NJ) using a buffer that consisted of 20 mM MOPS, 139 mM KCl, 12 mM NaCl, and 0.1% (w/v) DPC (pH 7.3), and the eluted protein was concentrated by ultrafiltration. These syb samples in DPC were typically at protein concentrations of 50−200 μM and were used for EPR spectroscopy.

Bicelle samples containing syb for EPR were prepared by first reconstituting the protein into DMPC (Avanti Polar Lipids, Alabaster, AL). The lipid in chloroform was dried under vacuum to produce a film of DMPC, and this sample was rehydrated with 20 mM MOPS, 139 mM KCl, and 12 mM NaCl (pH 7.3). A specific volume of syb in DPC was then added to the lipid suspension, and the solution was then incubated overnight at 4 °C and dialyzed twice in 20 mM MOPS, 139 mM KCl, and 12 mM NaCl (pH 7.3) to remove the detergent. The resulting vesicle suspension was spun down at 500000*g*, and the lipid concentration was evaluated by a phosphate assay. The desired amount of DHPC was then added to achieve the appropriate detergent:lipid ratio, and the mixture was subjected to bath sonication for 20 min. The final protein concentration for EPR was 20−60 μM.

To prepare synaptobrevin in lipid vesicles, a POPC/POPS (3:1) suspension was prepared by drying the lipids in chloroform (Avanti Polar Lipids) into a film followed by hydration in a buffer that consisted of 20 mM MOPS, 139 mM KCl, and 12 mM NaCl (pH 7.3). Appropriate quantities of synaptobrevin in DPC were then added to the lipid mixture followed by incubation for 2 h at room temperature and dialysis against 20 mM MOPS, 139 mM KCl, and 12 mM NaCl (pH 7.3). Following removal of the detergent, the vesicles were pelleted by centrifugation at 500000*g* for 20 min. The protein:lipid ratio was approximately 1:1000, and the protein concentration was in the range of 40−100 μM.

For the continuous wave measurements, samples were loaded into glass capillaries with inner and outer diameters of 0.6 and 0.84 mm, respectively (VitroCom, Mountain Lakes, NJ). The measurements were performed on a Bruker EMX spectrometer with a room-temperature ER 4123D dielectric resonator using a 2 mW incident microwave power and a 1 G modulation amplitude. Amplitudes for the EPR spectra were taken from spectra normalized by spin number. The power saturation experiments were performed on Bruker EMX as described elsewhere,[23] except the NiEDDA concentration was kept at 10 mM. All EPR spectra and data were processed using LabView programs provided by C. Altenbach (University of California, Los Angeles, CA).

Simulations of EPR spectra to obtain motional rates for the nitroxide, motional populations, and hyperfine coupling constants were conducted using a LabView program, Multi-Component, provided by C. Altenbach. This program implements a program for fitting slow motional EPR spectra written by Freed and co-workers.[24] The spectra were adequately fit by assuming the presence of two motional components having isotropic rates. The initial magnetic parameters used in the fits were taken from those obtained previously for R1 on aqueous exposed helical sites.[25]

RESULTS

Synaptobrevin Has a Different Structure in Bicelles and Micelles. To compare the structure of rat synaptobrevin 2 (syb) in micelle and bicelle environments, we obtained two-dimensional HN TROSY spectra of syb in small (q = 0.33) bicelles (Figure 1b). This bicelle environment yielded spectra

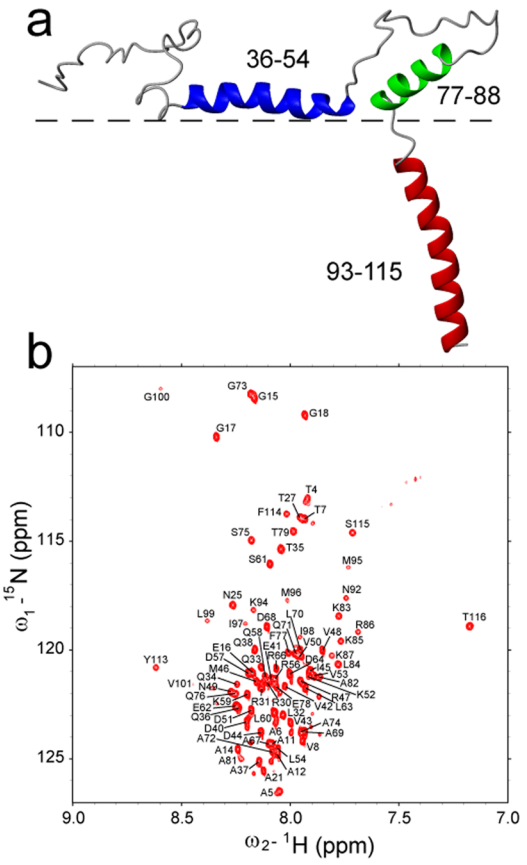

Figure 1. (a) Model obtained previously by solution NMR in DPC micelles for full-length synaptobrevin (Protein Data Bank entry 2KOG).[8] Three segments of the protein assume a helical structure: the transmembrane segment (residues 93−115, red), the juxtamembrane coupling helix (residues 77−88, green), and the N-terminal half of the SNARE motif (residues 36−54, blue). (b) ^{15}N−^{1}H HSQC NMR spectrum of Syb(1−116) in DMPC/DHPC (q = 0.33) bicelles at 40 °C (66 mM DMPC and 200 mM DHPC).

having a resolution and a signal-to-noise ratio similar to those previously obtained for syb in DPC micelles.[8] The spectra in bicelles were reassigned using ^{2}H-, ^{13}C-, and ^{15}N-labeled samples and similar strategies as previously described for the DPC samples.[8] The assignments are shown in Figure 1b. The protein secondary structure was semiquantitatively assessed by examining the difference between secondary Cα and Cβ chemical shifts as described previously,[17] and Figure 2 shows a comparison between the secondary Cα − Cβ shift differences for syb in DPC and bicelles. While the chemical shifts in the TM and coupling helices were similar in micelles and bicelles, shift differences of ≥2 ppm are observed for syb in DPC in the region of residues 37−53, indicating the presence of an α-helical structure; however, the same region in bicelles displays secondary Cα − Cβ differences of ≤1 ppm and is consistent with random coil structure. This finding is generally consistent with an NMR study in nanodiscs indicating that syb has a

dx.doi.org/10.1021/bi401638u | *Biochemistry* 2014, 53, 1485−1494

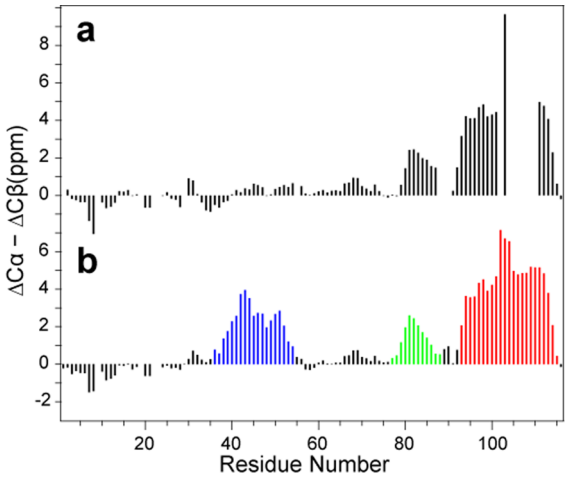

Figure 2. Chemical shift index obtained from Cα and Cβ resonances for syb in (a) DMPC/DHPC bicelles (q = 0.33) and (b) DPC micelles.

random coil structure in the SNARE motif, although signals in the coupling and TM helices were not resolved in this study.[9] Several resonances in the C-terminal half of the transmembrane helix that are resolved in DPC are not resolved in bicelles.

More quantitative methods for determining secondary structure from chemical shifts have been devised,[26,27] and they yield results similar to those shown in Figure 2. Here, backbone HN, Cα, CO, and N and side chain Cβ chemical shifts were used with the delta2D method[26] and are shown in Figure S1 of the Supporting Information. While the method suggests that syb in bicelles is largely random coil, the analysis indicates that a small (<10%) amount of helix may be present at and near residue 45 in bicelles, and that there may be a small (<20%), short stretch (three to five residues) of helix at and near residue 30 that is not seen in micelles or in solution. Thus, while the region encompassing residues 37−53 shows a greater propensity for helical structure in DPC micelles than in low-q bicelles, the delta2D method suggests that a small helical population may be in equilibrium with a random coil structure in some regions of synaptobrevin.

^{15}N Spin Relaxation Reveals Conformational Exchange in Regions of Bicelle-Bound Synaptobrevin. Nuclear spin relaxation rates are sensitive to local order and dynamics, and ^{15}N spin−lattice (R_1) and spin−spin (R_2) relaxation rates were measured in bicelles (q = 0.33) to explore the dynamics of syb. As shown in Figure 3a, elevated R_2/R_1 values are observed for residues 77−116, suggesting that there is a higher degree of local order and/or a shift in spectral density to lower frequency compared to those of residues 1−25. This is consistent with the known random coil structure of residues 1−25 and the α-helical structure of most residues in the region of residues 77−116, which are in the proximity of or inserted into the bicelle. Residues 37−54 also exhibit R_2/R_1 values that are elevated relative to those of residues 1−25 but R_2/R_1 values smaller than those observed for the transmembrane α-helix (residues 93−115). In contrast, the rest of SNARE motif residues 55−76 showed relatively small R_2/R_1 values, similar to that of residues 1−25. These R_2/R_1 values are consistent with a model for the region of residues 37−54 in which a small population of syb assumes an α-helical form and/or is interacting with the bicelle. To test for exchange, the dependence of the ^{15}N R_2 on the refocusing pulse repetition

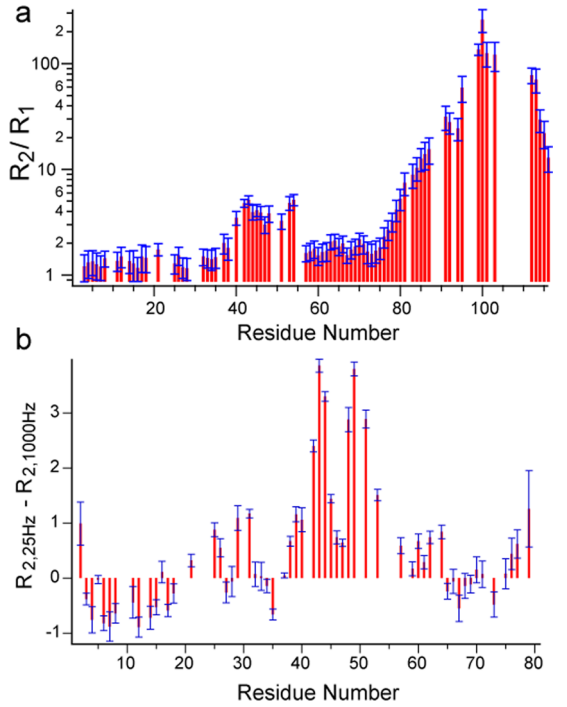

Figure 3. (a) Ratio of ^{15}N R_2/R_1 relaxation rates plotted for syb(1−116) in small DMPC/DHPC bicelles (q = 0.33) measured at 40 °C and 800 MHz. (b) Change in the spin−spin relaxation rates at two extreme CMPG pulse frequencies of 25 and 1000 Hz, measured at 25 °C and 800 MHz, for syb(1−116) in DMPC/DHPC bicelles (q = 0.5).

rate (relaxation dispersion) for syb in bicelles was examined and is shown in Figure 3b. Additional relaxation dispersion data at lower temperatures are shown in Figure S2 of the Supporting Information. The observed dependence of the ^{15}N spin−spin relaxation rate on CPMG pulse spacing for several residues between positions 42 and 52 indicates that these residues undergo conformational (random coil−α-helical transitions) and/or environmental exchange (binding on and off the bicelle). The small difference in R_2 values obtained for the different CPMG frequencies suggests that the exchange process is relatively fast (about 10^5 s^{-1}). Unfortunately, the small amplitude of the relaxation dispersion precluded a more detailed quantitative analysis of the dynamics.

EPR Spectra of Synaptobrevin Are a Result of Two Motional Components That Vary as a Function of the Curvature of the Environment. To examine the configuration and dynamics of synaptobrevin on lipid bilayers, the native cysteine at position 103 was mutated to alanine, and 21 sites in the SNARE motif were labeled with the spin-labeled side chain R1 (see Figure 4a). Shown in Figure 4b are representative EPR spectra from synaptobrevin in which the R1 side chain is placed at the indicated position. These spectra, which have been normalized by total spin number, are shown for the protein incorporated into POPC/POPS bilayers and DPC micelles. A complete set of EPR spectra are provided in Figure S3 of the Supporting Information. To provide a relative measure of the mobility of the R1 side chain along synaptobrevin, the peak-to-peak amplitudes are plotted in Figure 4c for the syb R1 mutants in bilayers and DPC micelles.

Two features are immediately obvious from the EPR spectra shown in Figure 4 (and Figure S3 of the Supporting Information). First, the normalized amplitudes in DPC are

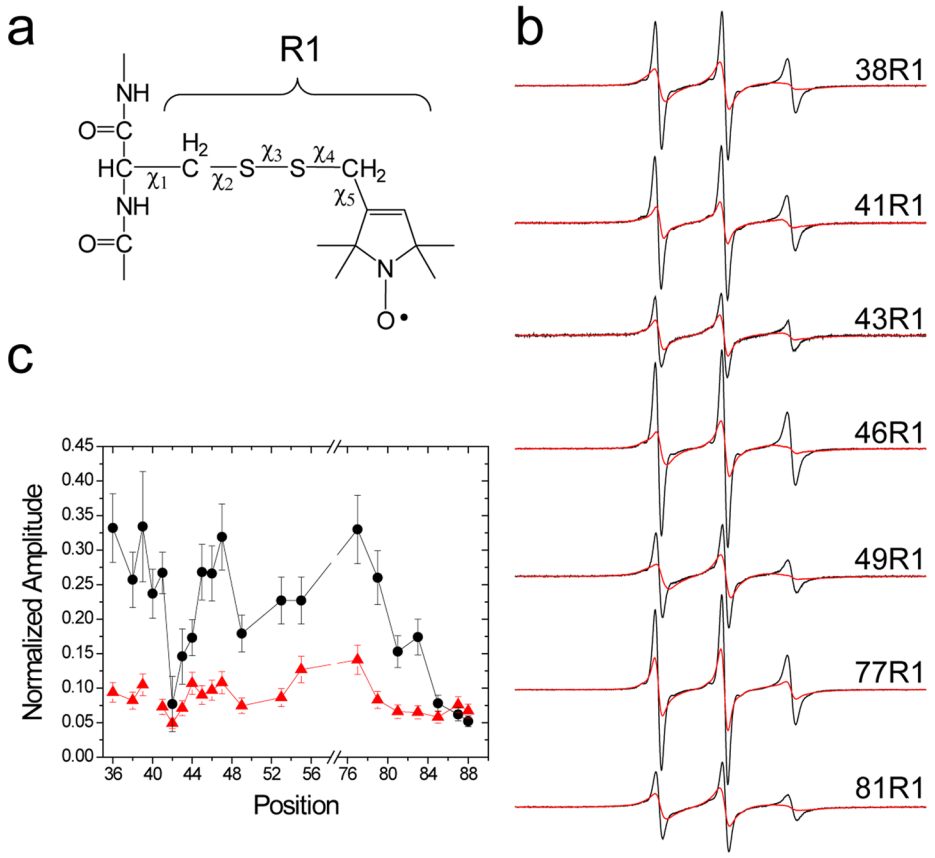

Figure 4. (a) Spin-labeled side chain R1 produced by the reaction of the MTSL reagent with a cysteine side chain. For this label, there are in principle five rotatable bonds linking the spin-label to the protein backbone; however, under most conditions, motion about X_1–X_3 is limited. (b) Selected normalized X-band EPR spectra from the spin-labeled sites within the SNARE motif of rat synaptobrevin 2 reconstituted into either POPC/POPS (3:1) bilayers (black trace) or docecylphosphocholine micelles (red trace). Spectra are all 100 G scans. (c) Normalized amplitudes of the EPR spectra as a function of position along synaptobrevin 2. These amplitudes provide a relative measure of the motional averaging of the R1 side chain where the more motionally averaged side chains have the highest intensities.

dramatically different from those in bilayers and indicate that that motion of the spin-labeled side chain is slowed in DPC. Second, there is considerable variation in the amplitudes of the synaptobrevin spectra as a function of position in the POPC/POPS sample. Sites 42–44 as well as site 49 show intensities significantly lower than those at other positions on the SNARE motif. At a minimum, this indicates that the SNARE motif in syb is not uniformly unstructured in the presence of lipid bilayers. Sites 81–88 also have lower intensities, and this is likely due to membrane insertion of the region adjacent to the TM domain.[28]

The EPR spectra for the SNARE motif in bilayers appear to be highly mobile and indicative of an unstructured protein segment. This is at first glance consistent with the recent NMR results for synaptobrevin in nanodiscs[9] as well as an earlier EPR study on synaptobrevin in bilayers.[28] However, a closer examination of the EPR line shapes indicates that they are composed of at least two motional components. Shown in Figure 5a are EPR spectra for sites 49 and 85 and fits using an EPR simulation package based upon the MOMD approach developed by Freed and co-workers (see Experimental Procedures). For these spectra, the simulations required two motional components to obtain a reasonable fit but were not improved by including an additional motional component. Shown in Figure 5b are the two components required for the fits shown in Figure 5a. The correlation times and fractions of the two components that reproduce the spectra are given in the

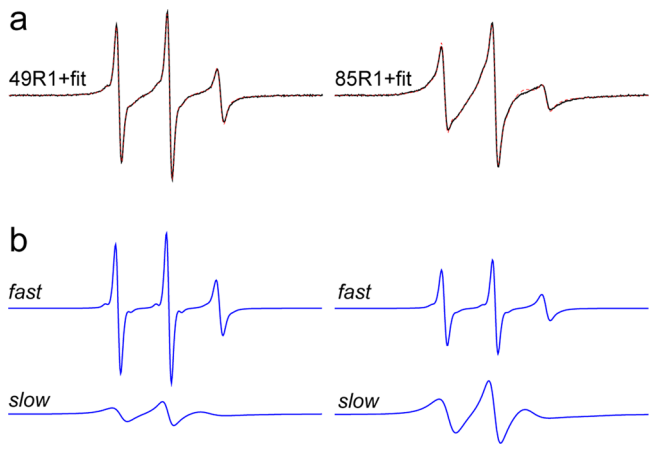

Figure 5. (a) EPR spectra for 49R1 and 85R1 in POPC/POPS bicelles (black trace) along with simulations (red dashed lines) that reproduce these spectra. (b) Spectra corresponding to the fast and slow components that when added produce the simulations shown in panel a for positions 49 and 85. For 49R1, the fast and slow components have correlation times of 0.44 and 2.7 ns, respectively, which are at relative spin populations of 45 and 55%, respectively. For 85R1, the fast and slow components have correlation times of 0.65 and 3.1 ns, respectively, which are at relative spin populations of 20 and 80%, respectively.

dx.doi.org/10.1021/bi401638u | *Biochemistry* 2014, 53, 1485–1494

legend. The fast motional component in these spectra is consistent with that expected for an unstructured segment that lies in the aqueous phase, and the slower motional component is similar to spectra obtained from peptides that are associated with the membrane−solution interface.[29,30] The variation in the normalized amplitude along the SNARE motif of synaptobrevin (Figure 4c) results in part from differences in these two motional populations, so that the sites having the largest fraction of the slower-moving component have the lowest amplitudes. The differences between bilayers and DPC also result from a greater population of the slow motional component in the micelle system (see below).

In addition to bilayer and micelle environments, spectra for several of these spin-labeled mutants were obtained in DHPC/DMPC bicelles to provide a direct comparison with the NMR data shown above. The normalized EPR spectra in lipid bilayers and in q = 2 and q = 0.4 bicelles are shown in Figure S4 of the Supporting Information. In almost every case examined, the spectra in lipid have the highest normalized intensities, followed by the q = 2 and q = 0.4 bicelles. The EPR spectra obtained in bilayers, bicelles, and micelles were simulated, and the parameters for each component were averaged across multiple positions in the SNARE motif (legend of Figure 6). The resulting values of the A_{zz} component of the hyperfine tensor, the correlation time, and the population of each component are shown in Figure 6. The average correlation times for the more mobile components were between 0.4 and 0.7 ns, and average A_{zz} values were between 36.2 and 36.9 G; these correlation times and A_{zz} values, which are sensitive to polarity, indicate that the protein is unstructured and in an aqueous environment.[31] The values of A_{zz} obtained for the slower component are consistent with an interfacial or hydrocarbon location for the R1 side chain; however, EPR line shapes and correlation times are more difficult to interpret for hydrocarbon-facing labels,[32,33] and the slower component might arise from an unstructured and/or helical backbone segment.

Remarkably, the correlation times of the two components do not significantly change when bilayer, bicelle, and micelle environments are examined (Figure 6b), but as indicated in Figure 6c, the populations of the two components change as a function of environment, so that the population of the slower-moving component is largest in DPC micelles and smallest in bilayers. These EPR spectra are consistent with exchange of the labeled syb on and off the interface at a rate that is slower than the EPR time scale ($<10^8$ s^{-1}). It should be noted that in addition to measurements in bilayers formed by POPC and POPS, several sites (36, 43, and 53) were also examined in bilayers formed from POPC, which yields a neutral bilayer interface. These spectra, which are shown in Figure S5 of the Supporting Information, were not altered by the absence of POPS, indicating that the membrane surface potential or surface charge density does not play a strong role in controlling the partitioning of the SNARE segment of syb.

The syb EPR spectra were power-saturated in the presence of O_2 or Ni(II)EDDA to assess the local environment of the spin-labeled Syb in bilayers.[34] Spin-label depth parameter φ is shown in Figure S6 of the Supporting Information as a function of label position. The depth parameter measurement will be dominated by the shorter correlation time component of the spectra because of the large amplitude and small line width of this component. Depth parameters for positions between 36 and 83 indicate a high degree of aqueous exposure with little bilayer contact, and this is consistent with an aqueous

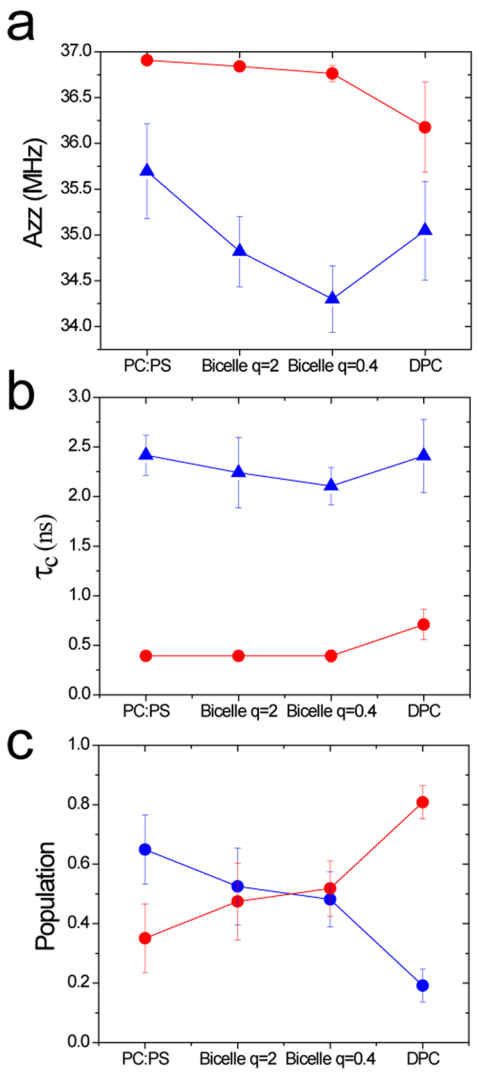

Figure 6. EPR parameters obtained from two-component fits such as those shown in Figure 5. (a) Values of the hyperfine coupling constant, A_{zz}, required to fit the fast (red) and slow (blue) motional components in the EPR spectra in PC/PS bilayers, q = 2 DMPC/DHPC bicelles, q = 0.33 DMPC/DHPC bicelles, and DPC micelles. (b) Values of the rotational correlation time, τ_c, required to fit the fast (red) and slow (blue) motional components in each environment. (c) Relative populations of the fast (red) and slow (blue) motional components required to fit the spectra in each environment. The error bars indicate the variation in values across all positions for which spectra were simulated. Parameters for the two-component fit included 15 positions in bilayers, 14 positions in DPC, and 8 positions in bicelles. Results were not included for positions 42−44 in bilayers, which appear to be more strongly associated with the interface.

localization for the conformer giving rise to the fast component. The N-terminus of the syb transmembrane helix is at or near residue 92, and the increase in the depth parameter that appears to begin near residue 85 or 87 is consistent with the interfacial or hydrocarbon localization for this end of the SNARE segment that was seen previously by using EPR spectroscopy.[28]

These data demonstrate that differences in EPR spectra along the length of the SNARE motif as well as the differences among bilayer, bicelle, and micelle environments are a result of a shift in the populations of fast and slow motional components that are associated with aqueous and interfacial localization,

dx.doi.org/10.1021/bi401638u | Biochemistry 2014, 53, 1485−1494

respectively. The result indicates that the SNARE motif of synaptobrevin partitions between aqueous and interfacial locations, and that this partitioning is a function of the membrane or membrane mimetic system and the interfacial environment. The increase in the interfacial population as one proceeds from bilayer to bicelle to micelle phases suggests that the tendency of the SNARE motif to transiently associate is correlated with the curvature of the interface.

DISCUSSION

Previous work on full-length synaptobrevin indicated that the SNARE motif is unstructured in bilayers or bilayer-like environments, and it has been suggested that the interfacial association and helical content of this segment that are observed in micelles are artifacts of the micelle environment.[9] The work presented here reaches a somewhat different conclusion with regard to the state of the protein. The combination of NMR and EPR data indicates that membrane association and partial helical content for the SNARE motif of syb occur in every environment examined (bilayers to micelles) but do so to a greatly reduced extent as the interface becomes more planar. This dependence upon the curvature of the interface explains the differences observed by NMR among DPC,[8] bicelles, and nanodiscs.[9]

EPR spectroscopy is a good method for distinguishing conformational exchange events and populations of conformers,[35,36] and a careful examination of the EPR spectra from the SNARE-forming motif of syb reveals the presence of two motional components in every environment examined. These two components appear to arise from aqueous and membrane-associated protein, and the differences in the EPR spectra of syb in different interfacial environments are largely due to the populations of fast and slow motional components (Figure 6c). The slow component dominates the spectra from DPC micelles; the fast motion component dominates in phospholipid bilayers, and the two components make comparable contributions in bicelles. Similarly, the NMR data presented here in bicelles indicate that several residues, including residue 44 and nearby neighboring residues, are in exchange (Figure 3) and at least partially helical (Figure S1 of the Supporting Information), suggesting that the interfacial protein assumes a partial helical state. The highly resolved resonances in NMR and the two-component EPR spectra indicate that the rate at which the SNARE motif exchanges between aqueous and interfacial phases is slow on the EPR time scale but fast on the NMR time scale. This places the exchange rate in the range of 10^5–10^8 s^{-1}.

A model illustrating the equilibrium that would explain these data is shown in Figure 7. The slow components in the EPR spectra are best explained by the interfacial states (iii and iv in Figure 7a), and the fast component is due to the aqueous syb states (i and ii in Figure 7a). When syb is in solution, the unstructured form of syb is highly favored, as indicated by the fact that little helical content is detected for the SNARE motif of syb in the absence of an interface. The fraction of α-helical content found in the syb SNARE domain in DPC micelles and DHPC/DMPC bicelles by NMR (Figure 2b) roughly correlates with partitioning of the SNARE domain into the membrane mimetics observed by EPR, indicating that when the SNARE motif is associated with the interface, the helical form is strongly favored. However, this correlation is not always perfect. For example, when position 45 is examined in small DMPC/DHPC bicelles, the slow EPR component represents

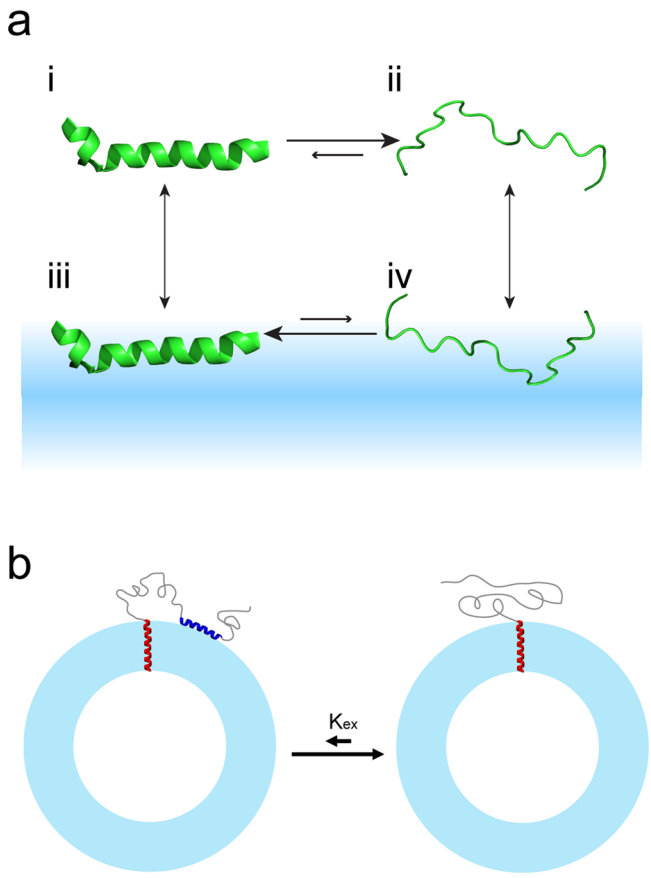

Figure 7. (a) Model based upon previous work[47] for the interfacial association of a helical segment that is in conformational exchange between folded (helical) and unfolded forms. In solution, the disordered form (ii) is favored relative to the helical form (i), while in the membrane, the equilibrium favors the helical form (iii) over the unfolded form (iv). (b) In the membrane, the equilibrium favors the unstructured aqueous form of the syb SNARE-forming segment; however, the SNARE-forming domain of syb samples the membrane and converts between helical and random forms, increasingly favoring the helical form in highly curved regions.

~50% of the total spins, while the population of helix determined by NMR is <10%. This difference might be a result of the spin-label or an indication that much of the bound component is not α-helical and that unstructured and α-helical forms coexist in the bound state.

An interesting observation revealed in the EPR spectra is that the fraction of protein associated with the interface increases as one moves from a bilayer to a bicelle to a micelle system (Figure 6c). Clearly, there are differences in the composition of these interfaces, including the lack of a glycerol backbone in the DPC micelle and the presence of unsaturated lipids in the bilayer phase. Conceivably, these differences might contribute to some of the differences that are observed. However, the differences in partitioning are correlated with the expected curvature of the interface in these systems, and this would appear to provide an explanation for the differences in helical content and partitioning. The SNARE domain has significant amphipathic character when it is α-helical,[8] and lipid interfaces will stabilize the helical form of these amphipathic sequences.[37−40] In addition, the interfacial insertion of an amphipathic α-helix will be favored by the presence of defects (exposed hydrophobic area) at the membrane mimetic interface.[41,42] The

dx.doi.org/10.1021/bi401638u | Biochemistry 2014, 53, 1485−1494

relative level of interfacial surface area containing a defect should decrease in the following order: DPC micelles > DHPC/DMPC bicelles > PC/PS bilayers. The same order is observed for partitioning of syb between aqueous and membrane mimetic phases (Figure 6c).

EPR data for selected sites in synaptobrevin were presented previously and are generally in agreement with the data obtained here.[28] The EPR line shapes are dominated by narrow lines indicative of an unstructured protein segment, and power saturation indicates that the segment adjacent to the transmembrane helical domain is buried within the bilayer. However, there are some important differences in the conclusions reached. As indicated here, a close examination of EPR line shapes and their variability with environment indicates that the SNARE motif of synaptobrevin is in equilibrium between the aqueous phase and the lipid interface. In addition, depth parameters near the transmembrane segment measured (Figure S6 of the Supporting Information) do not suggest the helical pattern observed previously; however, the error in these measurements is relatively large, and sites placed in this region were limited and were not the focus of this study.

Membrane fusion is triggered by interactions of syb with plasma membrane SNAREs to form a SNARE complex. This interaction will be facilitated by collisions with the acceptor complex and may be nucleated by helix formation as suggested previously;[43] as a result, the kinetics of SNARE complex formation is likely to depend on the equilibria shown in Figure 7a. It is easy to imagine how the membrane partitioning of the SNARE motif and helix−coil transitions within this region might modulate fusion. Aqueous states i and ii would be more likely to collide with aqueous acceptor SNAREs, but the membrane-associated syb (states iii and iv) could function as sites of nucleation for SNARE complex assembly, both because they tend to be more helical and because t-SNAREs such as syntaxin may also associate with interfaces.[44] As shown here, the curvature of the interface and the presence of membrane defects will alter the aqueous−membrane partitioning of syb and thereby modulate the availability of syb for SNARE complex formation. As a result, the lipid composition at the focal site of fusion and the presence of curvature or curvature strain are expected to influence the kinetics of SNARE complex formation. The calcium sensor synaptotagmin 1 has been reported to modulate membrane curvature,[45,46] and the observations made here indicate how synaptotagmin 1 might play a role in modulating the SNARE assembly indirectly by changing the properties of the bilayer.

In summary, we have used a combination of NMR and EPR spectroscopy to examine the partitioning and structure of the syb SNARE motif in different membrane mimetic environments. The syb SNARE domain associates with the lipid interface when bound to DPC micelles but favors the aqueous phase in the presence of PC/PS bilayers. When reconstituted into DHPC/DMPC bicelles, the syb SNARE domain partitions roughly equally between the solution and the interface. Even in lipid bilayers, a substantial fraction of the syb SNARE motif is associated with the interface, indicating that syb is not exclusively unstructured in the aqueous phase as an isolated SNARE protein. The tendency to associate with the membrane interface is correlated with the level of exposed hydrophobic surface area or defects that are expected in this environment. As a result, the state of syb is likely to be influenced by the specific lipid composition and curvature at the focal site of fusion.

■ ASSOCIATED CONTENT

Ⓢ Supporting Information

Five additional supplemental figures related to figures presented in the text. This material is available free of charge via the Internet at http://pubs.acs.org.

■ AUTHOR INFORMATION

Corresponding Authors

*E-mail: cafiso@virginia.edu. Telephone: (434) 924-3067. Fax: (434) 924-3567.

*E-mail: lkt2e@virginia.edu. Telephone: (434) 982-3578. Fax: (434) 243-8271.

Author Contributions

B.L. and D.D. contributed equally to this work.

Funding

This work was supported by National Institute of General Medical Sciences Grant GM072694.

Notes

The authors declare no competing financial interest.

■ ACKNOWLEDGMENTS

We thank Christian Altenbach (University of California, Los Angeles, CA) for providing LabView software for EPR data analysis and simulations.

■ ABBREVIATIONS

CPMG, Carr−Purcell−Meiboom−Gill; DHPC, dihexanoylphosphatidylcholine; DMPC, dimyristoylphosphatidylcholine; DPC, dodecylphosphocholine; EPR, electron paramagnetic resonance; MOMD, microscopic ordering with macroscopic disordering; MOPS, 3-(*N*-morpholino)propanesulfonic acid; MTSL, methanethiosulfonate spin-label; NiEDDA, nickel(II)−ethylenediamine-*N*,*N*′-diacetic acid complex; POPC, palmitoyloleoylphosphatidylcholine; POPS, palmitoyloleoylphosphatidylserine; R1, spin-labeled side chain produced by derivatization of a cysteine with MTSL; SDSL, site-directed spin labeling; SNAREs, soluble *N*-ethylmaleimide-sensitive factor attachment receptor proteins; syb, synaptobrevin 2; TROSY, transverse relaxation-optimized spectroscopy.

■ REFERENCES

(1) Hong, W. (2005) SNAREs and traffic. *Biochim. Biophys. Acta 1744*, 493−517.

(2) Jahn, R., and Scheller, R. H. (2006) SNAREs: Engines for membrane fusion. *Nat. Rev. 7*, 631−643.

(3) Carr, C. M., and Rizo, J. (2010) At the junction of SNARE and SM protein function. *Curr. Opin. Cell Biol. 22*, 488−495.

(4) Rizo, J., and Sudhof, T. C. (2002) Snares and Munc18 in synaptic vesicle fusion. *Nat. Rev. Neurosci. 3*, 641−653.

(5) Toonen, R. F., and Verhage, M. (2007) Munc18-1 in secretion: Lonely Munc joins SNARE team and takes control. *Trends Neurosci. 30*, 564−572.

(6) Hazzard, J., Sudhof, T. C., and Rizo, J. (1999) NMR analysis of the structure of synaptobrevin and of its interaction with syntaxin. *J. Biomol. NMR 14*, 203−207.

(7) Bowen, M., and Brunger, A. T. (2006) Conformation of the synaptobrevin transmembrane domain. *Proc. Natl. Acad. Sci. U.S.A. 103*, 8378−8383.

(8) Ellena, J. F., Liang, B., Wiktor, M., Stein, A., Cafiso, D. S., Jahn, R., and Tamm, L. K. (2009) Dynamic structure of lipid-bound synaptobrevin suggests a nucleation-propagation mechanism for trans-SNARE complex formation. *Proc. Natl. Acad. Sci. U.S.A. 106*, 20306−20311.

(9) Brewer, K. D., Li, W., Horne, B. E., and Rizo, J. (2011) Reluctance to membrane binding enables accessibility of the synaptobrevin SNARE motif for SNARE complex formation. *Proc. Natl. Acad. Sci. U.S.A. 108*, 12723−12728.
(10) Fasshauer, D., Eliason, W. K., Brunger, A. T., and Jahn, R. (1998) Identification of a minimal core of the synaptic SNARE complex sufficient for reversible assembly and disassembly. *Biochemistry 37*, 10354−10362.
(11) Schuette, C. G., Hatsuzawa, K., Margittai, M., Stein, A., Riedel, D., Kuster, P., Konig, M., Seidel, C., and Jahn, R. (2004) Determinants of liposome fusion mediated by synaptic SNARE proteins. *Proc. Natl. Acad. Sci. U.S.A. 101*, 2858−2863.
(12) Lee, D., Walter, K. F., Bruckner, A. K., Hilty, C., Becker, S., and Griesinger, C. (2008) Bilayer in small bicelles revealed by lipid-protein interactions using NMR spectroscopy. *J. Am. Chem. Soc. 130*, 13822−13823.
(13) Pervushin, K., Riek, R., Wider, G., and Wuthrich, K. (1997) Attenuated T-2 relaxation by mutual cancellation of dipole-dipole coupling and chemical shift anisotropy indicates an avenue to NMR structures of very large biological macromolecules in solution. *Proc. Natl. Acad. Sci. U.S.A. 94*, 12366−12371.
(14) Grzesiek, S., and Bax, A. (1992) Improved 3D triple-resonance NMR techniques applied to a 31-kDa protein. *J. Magn. Reson. 96*, 432−440.
(15) Wittekind, M., and Mueller, L. (1993) HNCACB, a high-sensitivity 3D NMR experiment to correlate amide-proton and nitrogen resonances with the α-carbon and β-carbon resonances in proteins. *J. Magn. Reson., Ser. B 101*, 201−205.
(16) Clubb, R. T., Thanabal, V., and Wagner, G. (1992) A constant-time 3-dimensional triple-resonance pulse scheme to correlate intraresidue H-1(N), N-15, and C-13(′) chemical-shifts in N-15-C-13-labeled proteins. *J. Magn. Reson. 97*, 213−217.
(17) Metzler, W. J., Constantine, K. L., Friedrichs, M. S., Bell, A. J., Ernst, E. G., Lavoie, T. B., and Mueller, L. (1993) Characterization of the three-dimensional solution structure of human profilin: ^{1}H, ^{13}C, and ^{15}N NMR assignments and global folding pattern. *Biochemistry 32*, 13818−13829.
(18) Kay, L. E., Torchia, D. A., and Bax, A. (1989) Backbone dynamics of proteins as studied by ^{15}N inverse detected heteronuclear NMR spectroscopy: Application to staphylococcal nuclease. *Biochemistry 28*, 8972−8979.
(19) Loria, J. P., Rance, M., and Palmer, A. G., III (1999) A TROSY CPMG sequence for characterizing chemical exchange in large proteins. *J. Biomol. NMR 15*, 151−155.
(20) Mulder, F. A., Skrynnikov, N. R., Hon, B., Dahlquist, F. W., and Kay, L. E. (2001) Measurement of slow (μs−ms) time scale dynamics in protein side chains by ^{15}N relaxation dispersion NMR spectroscopy: Application to Asn and Gln residues in a cavity mutant of T4 lysozyme. *J. Am. Chem. Soc. 123*, 967−975.
(21) Delaglio, F., Grzesiek, S., Vuister, G. W., Zhu, G., Pfeifer, J., and Bax, A. (1995) NMRPipe: A multidimensional spectral processing system based on UNIX pipes. *J. Biomol. NMR 6*, 277−293.
(22) Goddard, T. D., and Kneller, D. G. (2006) *SPARKY 3*, University of California, San Francisco.
(23) Frazier, A. A., Wisner, M. A., Malmberg, N. J., Victor, K. G., Fanucci, G. E., Nalefski, E. A., Falke, J. J., and Cafiso, D. S. (2002) Membrane orientation and position of the C2 domain from cPLA2 by site-directed spin labeling. *Biochemistry 41*, 6282−6292.
(24) Budil, D. E., Lee, S., Saxena, S., and Freed, J. H. (1996) Nonlinear-least-squares analysis of slow-motion EPR spectra in one and two dimensions using a modified Levenberg-Marquardt algorithm. *J. Magn. Reson., Ser. A 120*, 155−189.
(25) Columbus, L., Kalai, T., Jeko, J., Hideg, K., and Hubbell, W. L. (2001) Molecular motion of spin labeled side chains in α-helices: Analysis by variation of side chain structure. *Biochemistry 40*, 3828−3846.
(26) Camilloni, C., De Simone, A., Vranken, W. F., and Vendruscolo, M. (2012) Determination of secondary structure populations in disordered states of proteins using nuclear magnetic resonance chemical shifts. *Biochemistry 51*, 2224−2231.
(27) Marsh, J. A., Singh, V. K., Jia, Z. C., and Forman-Kay, J. D. (2006) Sensitivity of secondary structure propensities to sequence differences between α- and γ-synuclein: Implications for fibrillation. *Protein Sci. 15*, 2795−2804.
(28) Kweon, D. H., Kim, C. S., and Shin, Y. K. (2003) Regulation of neuronal SNARE assembly by the membrane. *Nat. Struct. Biol. 10*, 440−447.
(29) Qin, Z., Wertz, S. L., Jacob, J., Savino, Y., and Cafiso, D. S. (1996) Defining protein-protein interactions using site-directed spin-labeling: The binding of protein kinase C substrates to calmodulin. *Biochemistry 35*, 13272−13276.
(30) Victor, K., Jacob, J., and Cafiso, D. S. (1999) Interactions controlling the membrane binding of basic protein domains: Phenylalanine and the attachment of the myristoylated alanine-rich C-kinase substrate protein to interfaces. *Biochemistry 38*, 12527−12536.
(31) Subczynski, W. K., Wisniewska, A., Yin, J. J., Hyde, J. S., and Kusumi, A. (1994) Hydrophobic Barriers of Lipid Bilayer-Membranes Formed by Reduction of Water Penetration by Alkyl Chain Unsaturation and Cholesterol. *Biochemistry 33*, 7670−7681.
(32) Freed, D. M., Horanyi, P. S., Wiener, M. C., and Cafiso, D. S. (2010) Conformational exchange in a membrane transport protein is altered in protein crystals. *Biophys. J. 99*, 1604−1610.
(33) Kroncke, B. M., Horanyi, P. S., and Columbus, L. (2010) Structural origins of nitroxide side chain dynamics on membrane protein α-helical sites. *Biochemistry 49*, 10045−10060.
(34) Altenbach, C., Greenhalgh, D. A., Khorana, H. G., and Hubbell, W. L. (1994) A collision gradient method to determine the immersion depth of nitroxides in lipid bilayers: Application to spin-labeled mutants of bacteriorhodopsin. *Proc. Natl. Acad. Sci. U.S.A. 91*, 1667−1671.
(35) Flores Jimenez, R. H., Do Cao, M. A., Kim, M., and Cafiso, D. S. (2010) Osmolytes modulate conformational exchange in solvent-exposed regions of membrane proteins. *Protein Sci. 19*, 269−278.
(36) Lopez, C. J., Oga, S., and Hubbell, W. L. (2012) Mapping molecular flexibility of proteins with site-directed spin labeling: A case study of myoglobin. *Biochemistry 51*, 6568−6583.
(37) Ladokhin, A. S., and White, S. H. (1999) Folding of amphipathic α-helices on membranes: Energetics of helix formation by melittin. *J. Mol. Biol. 285*, 1363−1369.
(38) Li, Y., Han, X., and Tamm, L. K. (2003) Thermodynamics of fusion peptide-membrane interactions. *Biochemistry 42*, 7245−7251.
(39) Seelig, J. (2004) Thermodynamics of lipid-peptide interactions. *Biochim. Biophys. Acta 1666*, 40−50.
(40) Drin, G., and Antonny, B. (2010) Amphipathic helices and membrane curvature. *FEBS Lett. 584*, 1840−1847.
(41) Vamparys, L., Gautier, R., Vanni, S., Bennett, W. F., Tieleman, D. P., Antonny, B., Etchebest, C., and Fuchs, P. F. (2013) Conical lipids in flat bilayers induce packing defects similar to that induced by positive curvature. *Biophys. J. 104*, 585−593.
(42) Vanni, S., Vamparys, L., Gautier, R., Drin, G., Etchebest, C., Fuchs, P. F., and Antonny, B. (2013) Amphipathic lipid packing sensor motifs: Probing bilayer defects with hydrophobic residues. *Biophys. J. 104*, 575−584.
(43) Steinmetz, M. O., Jelesarov, I., Matousek, W. M., Honnappa, S., Jahnke, W., Missimer, J. H., Frank, S., Alexandrescu, A. T., and Kammerer, R. A. (2007) Molecular basis of coiled-coil formation. *Proc. Natl. Acad. Sci. U.S.A. 104*, 7062−7067.
(44) Liang, B., Kiessling, V., and Tamm, L. K. (2013) Pre-fusion structure of syntaxin 1A suggests pathway for folding into neuronal trans-SNARE complex fusion intermediate. *Proc. Natl. Acad. Sci. U.S.A. 110*, 19384−19389.
(45) Martens, S., Kozlov, M. M., and McMahon, H. T. (2007) How synaptotagmin promotes membrane fusion. *Science 316*, 1205−1208.
(46) Lynch, K. L., Gerona, R. R., Kielar, D. M., Martens, S., McMahon, H. T., and Martin, T. F. (2008) Synaptotagmin-1 utilizes

membrane bending and SNARE binding to drive fusion pore expansion. *Mol. Biol. Cell 19*, 5093−5103.
(47) Andersson, M., Ulmschneider, J. P., Ulmschneider, M. B., and White, S. H. (2013) Conformational states of melittin at a bilayer interface. *Biophys. J. 104*, L12−L14.